

Chemical Science

Accepted Manuscript

This article can be cited before page numbers have been issued, to do this please use: A. Gerstner, M. Arrowsmith, M. Dietz, C. Mihm and H. Braunschweig, *Chem. Sci.*, 2026, DOI: 10.1039/D6SC02501C.



This is an Accepted Manuscript, which has been through the Royal Society of Chemistry peer review process and has been accepted for publication.

Accepted Manuscripts are published online shortly after acceptance, before technical editing, formatting and proof reading. Using this free service, authors can make their results available to the community, in citable form, before we publish the edited article. We will replace this Accepted Manuscript with the edited and formatted Advance Article as soon as it is available.

You can find more information about Accepted Manuscripts in the [Information for Authors](#).

Please note that technical editing may introduce minor changes to the text and/or graphics, which may alter content. The journal's standard [Terms & Conditions](#) and the [Ethical guidelines](#) still apply. In no event shall the Royal Society of Chemistry be held responsible for any errors or omissions in this Accepted Manuscript or any consequences arising from the use of any information it contains.

ARTICLE

Zerovalent transition-metal inverse-sandwich complexes of a diborataanthracene dianion

Alexander Gerstner,^{a,b} Merle Arrowsmith,^{a,b} Maximilian Dietz,^{a,b} Cornelius Mihm,^{a,b} Holger Braunschweig^{*a,b}Received 00th January 20xx,
Accepted 00th January 20xx

DOI: 10.1039/x0xx00000x

The 9,10-dihydro-9,10-diborataanthracene (9,10-DHDBA) 2,3,6,7,9,10-Me₆-9,10-DHDBA (**2**) reacted with 1 equiv. [(MeCN)₃Cr(CO)₃] to yield the unsymmetrical half-sandwich complex [(η⁶-**2**)Cr(CO)₃] (**2-Cr**), in which the Cr(CO)₃ unit binds exclusively to one DHDBA benzo ring. Reactions of **2** with 2 equiv. [(MeCN)₃M(CO)₃] (M = Cr, Mo, W) yielded the centrosymmetric slipped inverse-sandwich complexes [(μ-(η⁶,η⁶-**2**))M(CO)₃]₂ (**2-M**₂), in which each M(CO)₃ unit binds to one of the DHDBA benzo rings, one above and one below the DHDBA plane. The twofold reduction of **2** with Li sand afforded the corresponding diborataanthracene (DBA) dianion, isolated as the C₄B₂-bound inverse-sandwich dilithio complex [(μ-(η⁶,η⁶-**2**))Li(thf)₂]₂ (**3**). The latter reacted with 2 equiv. [(MeCN)₃Cr(CO)₃] (M = Cr, Mo) to yield the first stable zerovalent transition-metal inverse-sandwich complexes of a [9,10-DBA]²⁻ dianion, complexes [(μ-(η⁶,η⁶-**2**))M(CO)₃Li(thf)₃]₂ (**3-M**₂). All new compounds were characterised by multinuclear NMR, UV-vis and IR spectroscopy, and their solid-state structures ascertained by single-crystal X-ray diffraction analyses. Furthermore, DFT calculations provide insight into the electronic structure of the 9,10-DHDBA and [9,10-DBA]²⁻ fused ring systems, as well as metal-(DH)DBA bonding in the chromium complexes **2-Cr**, **2-Cr**₂ and **3-Cr**₂.

Introduction

More than seven decades after the landmark isolations of ferrocene, [(η⁵-C₅H₅)₂Fe], and the first bis(benzene) complex, [(η⁶-C₆H₆)₂Cr],¹ sandwich complexes (or metallocenes), in which the metal centre is wedged between two π carbocycles, have become ubiquitous in organometallic chemistry, and are still finding new applications in small-molecule activation,² catalysis,³ materials design,⁴ and even pharmaceutical compounds.⁵ While sandwich complexes are now known for nearly all the metals of the periodic table, inverse-sandwich complexes, in which the π carbocycle is wedged between two metal centres (Figure 1), are less well explored. The formation of stable inverse-sandwich complexes requires a particularly electron-rich, often highly reduced π ligand, capable of coordinating one metal centre on each side, such as the 6π-aromatic cyclobutadiene dianion [C₄H₄²⁻],⁶ the 8π-antiaromatic benzene dianion [C₆H₆²⁻],⁷ the 10π-aromatic benzene tetraanion [C₆H₆⁴⁻],⁸ or the 10π-aromatic cyclooctatetraene (COT) dianion [C₈H₈²⁻].⁹ As metal...arene bonding in these complexes is mostly ionic in nature, the vast majority of inverse-sandwich complexes involve the more Lewis-acidic s- and f-block metals, kinetic stabilisation being provided by bulky ligand

spheres shielding the metal centres and the highly reactive reduced arene.¹⁰

Excluding triple-decker complexes, in which the metal centres are additionally sandwiched by another arene (usually cyclopentadienyl (Cp⁻) or [COT]²⁻),¹¹ and complexes with only partial metal...arene binding, there are only a handful of non-d⁰-metal inverse-sandwich complexes. These include some β-diketiminato-stabilised V(I), Nb(III) and Cr(I) complexes (**I**, Figure 1),¹² two amidinate-chelated Cr(I) derivatives (**II**),¹³ and a series of monovalent Cr(I), Mn(I) and Fe(I) terphenyl complexes (**III**),¹⁴ all with neutral benzene or toluene as the η⁶,η⁶-bridging ligand. Importantly, there are no known solely CO-bearing transition-metal (TM) inverse-sandwich complexes of organic π carbocycles of the form [(μ-(η⁶,η⁶-arene))TM(CO)_n]₂, as the TM(CO)_n fragments are usually too electron-rich and insufficiently stabilised by the CO ligands.

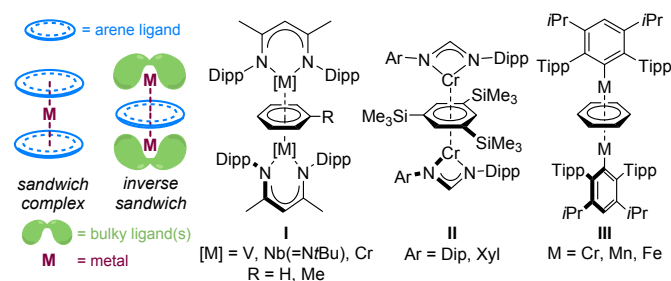


Figure 1. Examples of known non-d⁰ TM inverse-sandwich complexes. Dipp = 2,6-diisopropylphenyl; Tipp = 2,4,6-triisopropylphenyl; Xyl = 2,6-dimethylphenyl.

^a Institute for Inorganic Chemistry, Julius-Maximilians-Universität Würzburg, Am Hubland, 97074 Würzburg, Germany.

^b Institute for Sustainable Chemistry & Catalysis with Boron, Julius-Maximilians-Universität Würzburg, Am Hubland, Germany.

Electronic Supplementary Information (ESI) available: [details of any supplementary information available should be included here]. See DOI: 10.1039/x0xx00000x



The replacement of one or more endocyclic CR units by isoelectronic [BL] or [BR]⁻ units (L = neutral donor, R = anionic substituent) results in a dramatic increase in the electron-donating and π -acceptor ability of the resulting π boracycle compared to its all-carbon analogue, as the incorporation of the electropositive boron atom(s) raises the energy levels of the π -symmetry HOMOs while lowering that of the LUMO.¹⁵ Thus, monoanionic boratabenzenes, [C₅H₅BR]⁻, although isoelectronic to benzene, are much stronger donors, on a par with the Cp⁻ ligand,¹⁶ enabling the isolation of a wide array of d- and f-block (half)-sandwich and triple-decker complexes.¹⁷ Whereas benzene only forms sandwich and half-sandwich complexes with Cr(0), Fontaine reported the formation of the Cr(CO)₃ boratabenzene inverse-sandwich anion **IV** (Figure 2) as a byproduct in the synthesis of the piano-stool complex [η⁶-(2-SiMe₃-C₅H₄BCl)]Cr(CO)₃.¹⁸ Similarly, Herberich showed that a 4 π -antiaromatic borole enables the isolation of the Mn(CO)₃ inverse-sandwich complex **V**.¹⁹ Finally, borole dianions have been shown to be able to displace isoelectronic Cp⁻ ligands,²⁰ thus confirming their stronger donor ability.

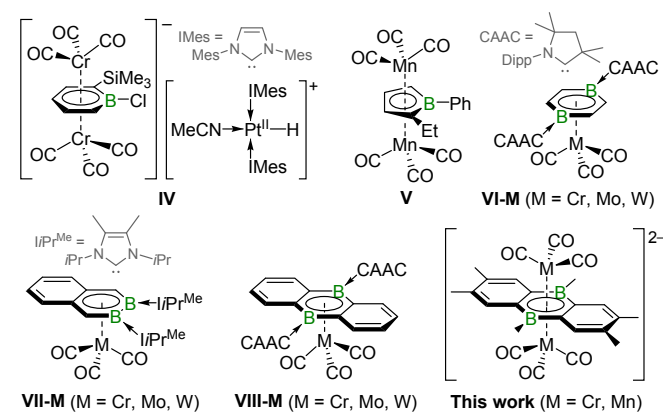


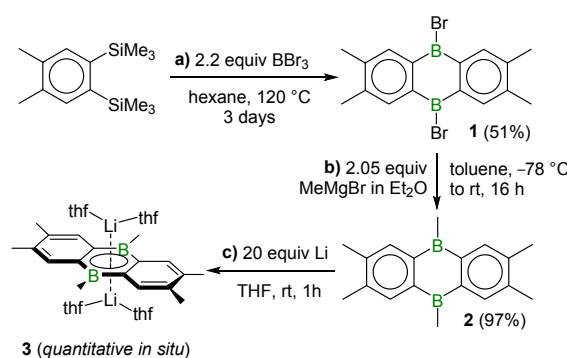
Figure 2. TM(CO)_n half- and inverse-sandwich complexes of π (di)boracycles.

The incorporation of two boron atoms into aromatic scaffolds generates even more powerful π ligands. Thus, we have shown that a neutral cyclic alkyl(amino)carbene (CAAC)-stabilised 1,4-diborabenzene (1,4-DBB) ligand is capable of stabilising zerovalent half-sandwich complexes of groups 6 (**VI-M**, M = Cr, Mo, W),²¹ 8 (M(CO)₂, M = Fe, Ru),²² and 10 (M(CO), M = Ni).²³ Similarly, neutral diboraacenes like an N-heterocyclic carbene (NHC)-stabilised 2,3-diboranaphthalene and a CAAC-stabilised 9,10-diboraanthracene (9,10-DBA) have enabled the isolation of the zerovalent group 6 half-sandwich complexes **VII-M** and **VIII-M** (M = Cr, Mo, W), respectively.^{24,25} However, no inverse-sandwich formation has ever been observed with these neutral diboraacenes. Our attention therefore turned to dianionic diboraacenes, which are obtained by the twofold reduction of neutral dihydrodiboraacene precursors,²⁶ and are known to form sandwich and triple-decker complexes with a small number of d- and f-block metals.²⁷ Herein, we report the synthesis of the mono- and bimetallic zerovalent group 6 complexes of a neutral 9,10-dihydro-9,10-diboraanthracene (9,10-DHDBA) and the first TM inverse-sandwich complexes of its 9,10-diboraanthracene dianion ([9,10-DBA]²⁻).

Results and discussion

Synthesis of (DH)DBA group 6 complexes

The dibromo precursor **1** was synthesised in a manner analogous to its non-methylated analogue²⁹ by heating a 1:2:2 mixture of 1,2-bis(trimethylsilyl)-4,5-dimethylbenzene and BBr₃ in hexane in a sealed thick-walled flask at 120 °C for days (Scheme 1a).[‡] Subsequent methylation with MeMgBr yielded 2,3,6,7,9,10-Me₆-9,10-DHDBA (**2**) in near-quantitative yield (Scheme 1b). The ¹¹B NMR shifts in C₆D₆ of **1** and **2** at 62.5 and 67.2 ppm, respectively, as well as their structural parameters (see Figures S61 and S62 in the ESI) are in agreement with those reported for their non-methylated analogues.^{28,29} It is noteworthy that in THF, the ¹¹B NMR resonance of compound **2** is upfield-shifted to 58.3 ppm, presumably owing to slow reversible THF coordination to the Lewis-acidic boron centres on the NMR timescale.



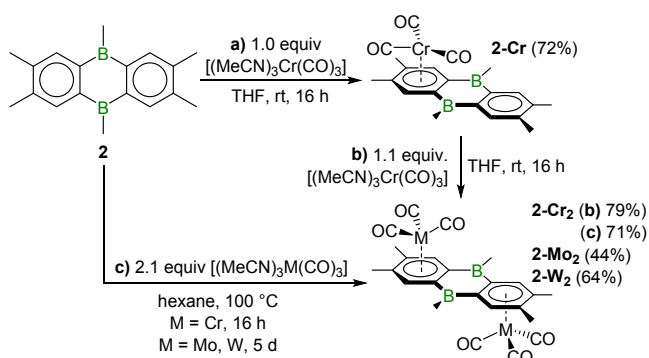
Scheme 1. Synthesis and two-electron-reduction of **2**.

The cyclovoltammogram of **2** in THF shows a reversible reduction wave at $E_{1/2} = -2.06$ V and an irreversible one at $E^{pc} = -2.71$ V (see Figure S61 in the ESI). The chemical two-electron reduction of **2** with a large excess of lithium sand in d₈-THF resulted in an instant colour change to pink, then dark red, and the appearance of a new broad ¹¹B NMR resonance at 22.0 ppm, identical to that of the parent [9,10-DBA]²⁻ and the [9,10-Me₂-9,10-DBA]²⁻ dilithio complexes (Scheme 1c).^{26a,30} The UV-vis spectrum of **3** in THF shows a major absorption at 436 nm with a shoulder at 415 nm, as well as two very broad, low-intensity bands, overlapping in the 500-600 nm region (Figure 3c). These are slightly redshifted compared to those of the parent [9,10-DBA][Li(thf)₂]₂ complex ($\lambda_{max} = 420$ nm, $\lambda_2 = 400$ nm, $\lambda_3 = 500$ nm).^{26a} While single crystals of complex **3** suitable for X-ray diffraction analysis could be isolated (see **X-ray crystallographic analyses**), the compound was not indefinitely stable in the solid state.

The 1:1 reaction of [(MeCN)₃Cr(CO)₃] and **2** in THF at rt led to the formation of the monometallic half-sandwich complex **2-Cr**, isolated as a red crystalline solid in 72% yield (Scheme 2a). In d₈-THF the broad ¹¹B NMR resonance of **2-Cr** at 46.3 ppm is significantly upfield-shifted compared to that of **2** ($\delta_{11B} = 58.3$ ppm). In benzene, however, in which **2-Cr** is only poorly soluble, its ¹¹B NMR resonance shifts back downfield to 64.9 ppm, 6 ppm upfield of the known unsymmetrical Cr(CO)₃ complex of 9,10-Me₂-9,10-DHDBA ($\delta_{11B} = 71$ ppm in C₆D₆).³¹ The larger upfield-



shift of the ^{11}B NMR resonance of **2-Cr** upon switching from benzene to THF ($\Delta\delta \approx -19$ ppm) compared to **2** ($\Delta\delta \approx -9$ ppm) suggests that the boron centres in **2-Cr** bind THF more strongly and are therefore more Lewis acidic.



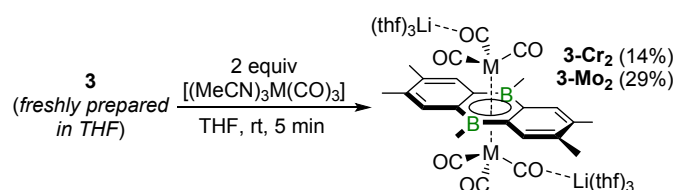
Scheme 2. Synthesis of mono- and bimetallic group 6 complexes of **2**.

In the ^1H NMR spectrum, two 2H singlets for the benzo protons, one of which is upfield-shifted to 5.83 ppm due to chromium coordination, reflect the unsymmetrical nature of **2-Cr**. The $^{13}\text{C}\{^1\text{H}\}$ NMR spectrum shows a single CO resonance at 234.5 ppm, ca. 22 ppm downfield-shifted from those of its 9,10-Me₂-DHDBA analogue ($\delta_{13\text{C}} = 212.8, 212.2$ ppm),³¹ indicating that the Cr(CO)₃ moiety rotates freely in solution. It is noteworthy that the coordination to the 9,10-DHDBA benzo ring is unique to the group 6 metals, as all other zerovalent TMs (Fe⁰, Ru⁰, Co⁰, Rh⁰, Ni⁰, Pd⁰, Pt⁰) preferentially coordinate to the central 1,4-diboro-2,5-cyclohexadiene ring.^{31,32}

The addition of a further equivalent of [(MeCN)₃Cr(CO)₃] to **2-Cr** yielded the centrosymmetric slipped inverse-sandwich complex **2-Cr₂**, isolated as a red crystalline solid in 79% yield (Scheme 2b). The coordination of the second Cr(CO)₃ unit results in a small downfield shift of the ^{11}B NMR resonance to 49.1 ppm (THF). A single upfield-shifted benzo singlet (4H) at 5.86 ppm confirms the symmetrical nature of the complex. **2-Cr₂** could also be obtained directly from the 2:1 reaction of [(MeCN)₃Cr(CO)₃] and **2** in hexane at 100 °C in a pressurised Schlenk flask (Scheme 2c). Attempted 1:1 reactions of the heavier group 6 precursors [(MeCN)₃M(CO)₃] (M = Mo, W) and **2** did not afford the corresponding mononuclear complexes **2-M** but only a 1:1 mixture of bimetallic **2-M₂** and unreacted **2**, as determined by NMR-spectroscopy. These could be accessed selectively by 2:1 reactions in hexane at 100 °C in pressurised Schlenk flasks, yielding **2-Mo₂** and **2-W₂** as red crystalline solids in moderate yields of 44% and 64%, respectively (Scheme 2c). Both show an ^{11}B NMR resonance around 45 ppm, upfield-shifted from that of **2-Cr₂** ($\delta_{11\text{B}} = 49.1$ ppm). The ^{13}C NMR CO resonance of **2-M₂** experiences a marked upfield shift upon moving down group 6 ($\delta_{13\text{C}} = 234.6$ (**2-Cr₂**), 221.8 (**2-Mo₂**), 212.4 (**2-W₂**) ppm), with similar chemical shifts to those observed in the [(η^6 -mesitylene)M(CO)₃] series.³³ The solid-state IR spectra of **2-M₂** all display a sharp C=O stretching band around 1936-1944 cm⁻¹ and a very broad unresolved band covering the 1800-1875 cm⁻¹ range. Both are shifted to slightly lower wavenumbers compared to the parent benzene complexes [(η^6 -C₆H₆)M(CO)₃]

($\nu(\text{C=O})_{\text{solid-state}} = 1965\text{-}1971, 1845\text{-}1875$ cm⁻¹),³⁴ indicating slightly weaker C–O bonds. This suggests that the benzo rings of the 9,10-DHDBA ligand are slightly better overall donors than benzene.

All four 9,10-DHDBA complexes are red. The UV-vis spectra of **2-Cr** and **2-M₂** (M = Cr, Mo, W) all show an absorption maximum around $\lambda_{\text{max}} = 330\text{-}350$ nm, as well as two very broad, overlapping, medium-intensity bands in the $\lambda_2 = 415\text{-}430$ nm and $\lambda_3 = 470\text{-}500$ nm regions, the latter accounting for their red colour. Comparison of the mono- and bimetallic complexes **2-Cr** ($\lambda = 333, 423, 481$ nm) and **2-Cr₂** ($\lambda = 349, 431, 497$ nm) shows a small redshift for all three bands in the latter (Figure 3a). Comparison of the three **2-M₂** complexes (Figure 3b), shows a small blueshift upon moving from **2-Cr₂** ($\lambda = 349, 431, 497$ nm) to **2-Mo₂** ($\lambda = 336, 417, 464$ nm), and a very minor redshift of λ_2 and λ_3 upon moving from **2-Mo₂** to **2-W₂** ($\lambda = 334, 422, 469$ nm).



Scheme 3. Synthesis of zerovalent inverse-sandwich group 6 complexes of **3**.

Siebert reported that the reduction of his 9,10-Me₂-9,10-DHDBA analogue of **2-Cr** with potassium did not lead to the desired shift of the Cr(CO)₃ unit to the central C₄B₂ ring but rather to decomposition.³¹ We therefore decided to attempt the synthesis of inverse-sandwich complexes starting from the already doubly reduced complex **3**. The addition of 2 equiv. [(MeCN)₃Cr(CO)₃] (M = Cr, Mo, W) to a freshly prepared THF solution of **3** at rt led to the instant formation of dark suspensions. The ^{11}B NMR spectra of the reaction mixture showed the formation of several unidentified sp^3 -boron-containing species, as well as a broad resonance at 12 ppm, present in the Cr- and Mo-based reactions, but not in the W-based one. After filtration, removal of the solvent and washing of the solid residues with various solvents, **3-Cr₂** and **3-Mo₂** were isolated as yellow solids in rather poor yields of 14% and 29%, respectively (Scheme 3). It is noteworthy that once formed, **3-Cr₂** and **3-Mo₂** were indefinitely stable in solution at rt. In the case of the W-based reaction, no equivalent **3-W₂** complex was observed, and no other product could be identified. Carrying out the reactions at -78 °C yielded no improvement in their selectivity. To our knowledge, these are the first examples of zerovalent TM inverse-sandwich complexes of a diborataanthracene ligand. The only other known [9,10-DBA]²⁻ complexes beyond the alkali metals are the dilanthanide triple-decker complexes recently reported by Morena-Pineda and Roesky.^{27b}

The ^{11}B NMR resonance of **3-Cr₂** and **3-Mo₂** at ca. 12 ppm is 10 ppm upfield-shifted compared to **3** ($\delta_{11\text{B}} = 22$ ppm), indicating a significant increase in electron density at the boron centres from interaction with the electron-rich Cr(0) centres (see **DFT calculations**). The centrosymmetric nature of **3-M₂** was attested



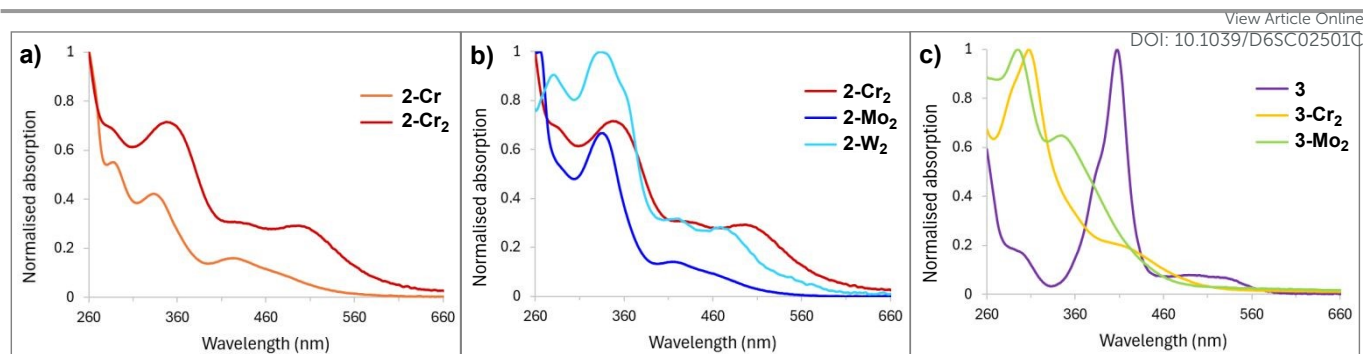
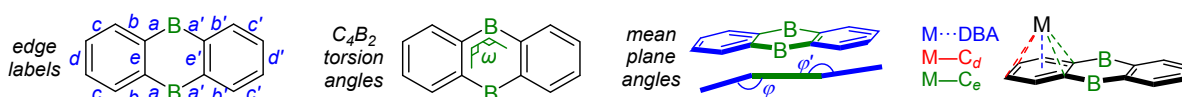


Figure 3. a-c) Overlays of the UV-vis spectra of the DHDBA and DBA metal complexes presented herein.

Table 1. ^{11}B NMR shifts (ppm) in d_8 -THF, and selected bond distances (\AA) and torsion angles ($^\circ$) of the crystallographically characterised compounds presented herein. $\overline{a/a'}$, $\overline{b/b'}$, $\overline{c/c'}$, $\overline{d/d'}$, $\overline{e/e'}$ = avg. edge length (see edge labels below); $\overline{M \cdots DBA}$ = avg. distance between the metal centre and the mean plane of the ring it coordinates to; $\overline{M - C_{d/e}}$ = avg. distance between the metal centre and the carbon atoms of the e/e' (and d/d') edges of the ring it coordinates to; $\overline{M - CO}$ = avg. metal–carbonyl bond lengths; $\overline{C - O}$ = avg. carbonyl C–O bond lengths; $|\omega_{\max}|$ = absolute value of the largest endocyclic torsion angle of the central B_2C_4 ring; ϕ = angle between the mean planes of the benzo and C_4B_2 rings.



	^{11}B NMR	$\overline{a/a'}$	$\overline{e/e'}$	$\overline{b/b'}$	$\overline{c/c'}$	$\overline{d/d'}$	$\overline{M \cdots DBA}$	$\overline{M - C_{d/e}}$	$\overline{M - CO}$	$\overline{C - O}$	$ \omega_{\max} $	ϕ/ϕ'
2	58.3	1.565(2)	1.419(2)	1.404(2)	1.395(2)	1.401(2)	–	–	–	–	10.6(2)	ca. 4.0
3	22.0	1.531(3)	1.472(3)	1.438(3)	1.370(3)	1.441(3)	ca. 1.87	2.385(4) ^c	–	–	1.1(3)	ca. 0.9
2-Cr	46.3	1.573(4), ^a 1.557(4) ^b	1.433(4), ^a 1.421(4) ^b	1.434(4), ^a 1.400(4) ^b	1.406(4), ^a 1.396(4) ^b	1.427(4), ^a 1.392(4) ^b	ca. 1.72	2.193(3), ^c 2.263(3) ^d	1.847(3)	1.156(4)	8.4(4)	ca. 5.2, ^a ca. 5.0 ^b
2-Cr₂	49.1	1.559(3)	1.451(3)	1.415(3)	1.421(3)	1.405(3)	ca. 1.71	2.201(2), ^c 2.263(2) ^d	1.853(3)	1.151(3)	2.5(3)	ca. 9.3
2-Mo₂	45.0	1.562(4)	1.450(4)	1.428(4)	1.403(4)	1.434(4)	ca. 1.88	2.316(3), ^c 2.400(3) ^d	1.984(3)	1.147(4)	6.3(4)	ca. 9.4
2-W₂	44.4	1.560(7)	1.444(6)	1.425(7)	1.415(7)	1.423(7)	ca. 1.87	2.311(2) ^c 2.390(6) ^d	1.964(7)	1.144(9)	8.9(6)	ca. 11.8
3-Cr₂^e	11.9	1.551(3)	1.457(2)	1.449(3)	1.355(3)	1.449(2)	ca. 1.78	2.287(2), 2.369(2) ^f	1.816(2), ^g 1.779(2) ^h	1.173(3), ^g 1.191(3) ^h	2.0(2)	ca. 2.3, ca. 0.8 ^f
3-Mo₂^e	12.0	1.557(9)	1.463(8)	1.448(9)	1.357(9)	1.443(9)	ca. 1.95	2.424(6), 2.500(6) ^f	1.931(7), ^g 1.889(10) ^h	1.173(9), ^g 1.197(10) ^h	1.6(8)	ca. 2.2, ca. 0.7 ^f

^a Within the metal-containing complex moiety; ^b within the metal-free complex moiety; ^c $\overline{M - C_{e/e'}}$; ^d $\overline{M - C_{d/d'}}$; ^e values provided for both molecules present in the asymmetric unit; ^f different avg. values measured for the e and e' edge; ^g for terminal CO ligands; ^h for Li-bound CO ligands.

by the single ^1H NMR benzo singlet (4H) at 7.45 ppm. In solution the $\text{Cr}(\text{CO})_3$ units rotate freely and the $[\text{Li}(\text{thf})_3]^+$ units fluctuate between all three CO ligands on the NMR timescale, as only one ^{13}C NMR carbonyl resonance is observed ($\delta_{^{13}\text{C}} = 242.0$ (**3-Cr₂**), 234.6 (**3-Mo₂**) ppm). The solid-state IR spectra reflect the presence of the Li-bound CO ligands through a series of stretching bands spanning the 1711–1935 cm^{-1} region, with the bands above 1850 cm^{-1} pertaining to the terminal CO ligands and those below 1800 cm^{-1} to those of the weaker Li-bound C=O bonds. As expected from the differences in colour, the UV-vis spectra of **3-M₂** (both yellow) differ greatly from that of their precursor **3** (red). Thus, **3-M₂** show only low-intensity absorptions around 440 nm, where **3** displays its λ_{\max} , and lack any bands in the 500–600 nm region (Figure 3c). Both their absorption maxima (**3-Cr₂** $\lambda = 308, 418$ nm; **3-Mo₂** $\lambda = 296, 344$ nm) are significantly blueshifted from those of **2-M₂**.

Furthermore, a blueshift is observed upon moving from **3-Cr₂** to the heavier **3-Mo₂**, as already noted between **2-Cr₂** and **2-Mo₂**.

X-ray crystallographic analyses

Compound 2. The central 1,4-dibora-2,5-cyclohexadiene ring of **2** is slightly bent along the $\text{B} \cdots \text{B}$ axis (ca. 7.8° , see Figure S63 in the ESI). The endocyclic B–C bond lengths (avg. 1.565(2) \AA) are typical for single bonds at sp^2 -hybridised boron. The C–C bonds of the outer b , c and d edges (see edges labelling in Table 1) show a relatively low degree of bond alternation (1.393(2)–1.406(2) \AA), with the ring junctions e being slightly elongated (1.419(2) \AA), indicating good π delocalisation over the benzo rings (see **DFT calculations**). Overall, these structural parameters are similar to those of the analogous 9,10-Me₂-9,10-DHDBA.²⁹

Complexes 2-M_n. Complexes **2-Cr** and **2-M₂** (M = Cr, Mo, W) all provided red single crystals suitable for SCXRD analyses. The



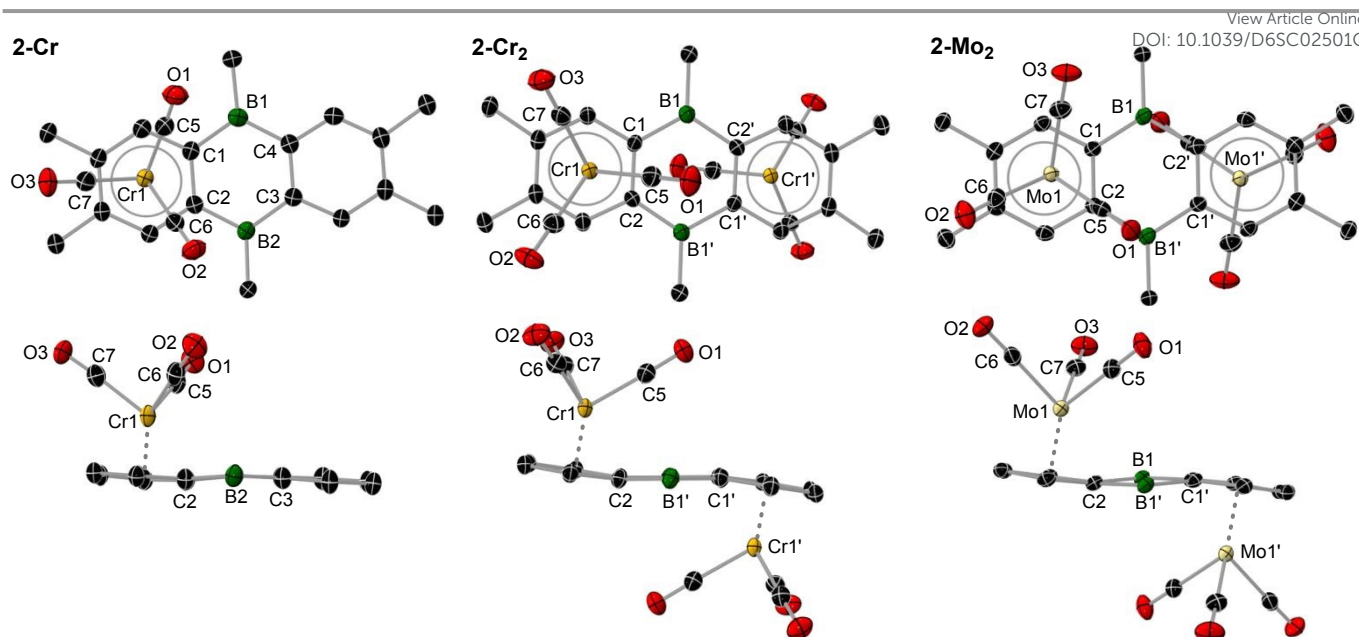


Figure 4. Crystallographically determined solid-state structures of **2-Cr**, **2-Cr₂** and **2-Mo₂**. Top: views from above the DHDBA plane, highlighting the various conformations of the M(CO)₃ moieties with respect to the DHDBA framework and to each other. Below: truncated views (methyl groups omitted) along the B...B axis, highlighting the bend of the DHDBA framework. Thermal displacement ellipsoids set at 50% probability. Hydrogen atoms omitted for clarity.

solid-state structure of **2-Cr** shows a single Cr(CO)₃ fragment η^6 -coordinated to one of the benzo rings (Cr...C₆ 1.72 Å, Figure 4, Table 1). In a similar manner, Cr(CO)₃ also coordinates to the outer ring of anthracene.³⁵ Metal coordination results in a small but significant (ca. 0.04 Å) lengthening of the *b* and *d* edges compared to the uncoordinated benzo ring. It is noteworthy that the Cr(CO)₃ is not centrally positioned above the benzo ring, but somewhat closer to the *e* than to the *d* edge (avg. Cr–C_e 2.193(3) Å; avg. Cr–C_d 2.263(3) Å, see explanation in **DFT calculations**). The Cr(CO)₃ fragment is staggered with respect to the benzo ring, one CO ligand pointing towards the *d* edge. The Cr–C_{CO} (1.843(3)–1.849(3) Å) and C–O (1.153(4)–1.157(4) Å) bond lengths show less variation than in the isostructural [η^6 -anthracene]Cr(CO)₃] complex (Cr–C 1.812(10)–1.834(10) Å; C–O (1.142(10)–1.184(12) Å).³⁵

In contrast to **2-Cr**, the three bimetallic complexes **2-M₂** are centrosymmetric, with one M(CO)₃ fragment η^6 -coordinated to each benzo ring, one above and one below the 9,10-DHDBA plane, in what may be called a slipped inverse-sandwich coordination mode (Figure 4, Table 1, see Figure S68 in the ESI for **2-W₂**). Whereas the central C₄B₂ ring in **2-Cr₂** is virtually planar ($|\omega_{\max}| = 2.5(3)^\circ$), it is slightly twisted in the two heavier analogues (**2-Mo₂** 6.3(4)°, **2-W₂** 8.9(6)°). Furthermore, all three complexes display a significant bend in the overall 9,10-DHDBA framework, the angle φ formed by the C₆ and C₄B₂ mean planes ranging from 9.3° to 11.8°. The endocyclic C–C and B–C bond lengths of all three dinuclear complexes are similar within the error of the measurement. The M...C₆ distance increases significantly from **2-Cr₂** (ca. 1.71 Å) to **2-Mo₂** (ca. 1.88 Å) but shows no further increase for **2-W₂** (ca. 1.87 Å). This is in line with the much lower difference between the hexacoordinate metallic radii of W and Mo, than of Mo and Cr (Cr 1.285, Mo

1.402, W 1.410 Å),³⁶ owed to the f-orbital contraction in W. These M...C₆ distances are all slightly shorter than those found in the [η^6 -C₆H₆]M(CO)₃] series (Cr 1.72, Mo 1.91, W 1.90 Å),³⁷ suggesting stronger metal...arene bonding. Complexes **2-M₂** display the same slightly unsymmetrical positioning of the metal centres above the C₆ rings as **2-Cr**, the M–C_d bonds being ca. 3% longer than the M–C_e bonds, owing to the influence of the fused electron-poor C₄B₂ ring (see **DFT calculations**). Whereas the M(CO)₃ fragments in **2-Cr₂** are staggered with respect to the benzo rings, this time with one CO ligand each pointing towards the central C₄B₂ ring, those in **2-Mo₂** and **2-W₂** are nearly eclipsed. These conformational differences may be at the origin of the differing degrees of distortion from planarity observed in their C₄B₂ rings (*vide supra*). Finally, the C–O bond lengths of all three complexes are statistically similar, in line with their very similar IR C–O stretching bands (*vide supra*).

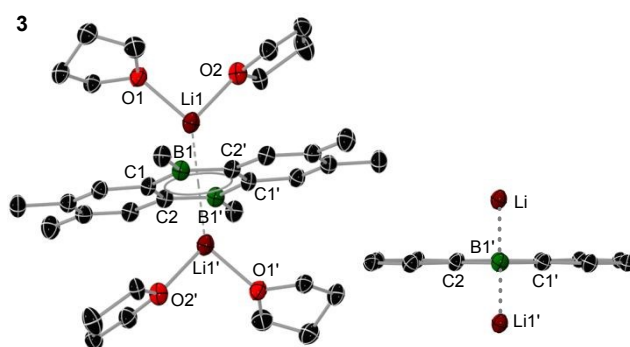


Figure 5. Left: crystallographically determined solid-state structure of **3**. Right: truncated view of **3** (methyl groups and THF ligands omitted) along the B...B axis, highlighting the planarity of the DBA framework. Thermal displacement ellipsoids set at 50% probability. Hydrogen atoms omitted for clarity.



Complex 3. While complex **3** was too sensitive to be isolated in bulk, recrystallisation by diffusion of hexane into a saturated THF solution at $-30\text{ }^{\circ}\text{C}$ yielded red crystals suitable for SCXRD analysis. The solid-state structure of **3** is centrosymmetric and shows an inverse-sandwich complex, with the lithium cations sitting atop and below the centre of the central B_2C_4 ring ($\text{Li}\cdots\text{B}_2\text{C}_4$ ca. 1.87 \AA), each coordinated by two THF molecules (Figure 5, Table 1). The aromatisation of the B_2C_4 ring is seen in the shortening of its endocyclic B–C bonds (**3** $1.531(3)$; **2** $1.565(2)\text{ \AA}$), the substantial lengthening of its C–C bonds (**3** $1.472(3)$; **2** $1.419(2)\text{ \AA}$), and its higher degree of planarity compared to **2** ($|\omega_{\text{max}}|$: **3** $1.1(3)$; **2** $10.6(2)^{\circ}$). Conversely, the fused benzo rings become less aromatic, now approaching alternating C–C single ($1.438(3)$, $1.441(3)\text{ \AA}$) and double ($1.370(3)\text{ \AA}$) bonds. Furthermore, the entire DBA framework is now virtually planar ($\varphi < 1^{\circ}$). These bonding parameters are similar to those found in other inverse-sandwich [9,10-DBA] Li_2 complexes.^{26a,38}

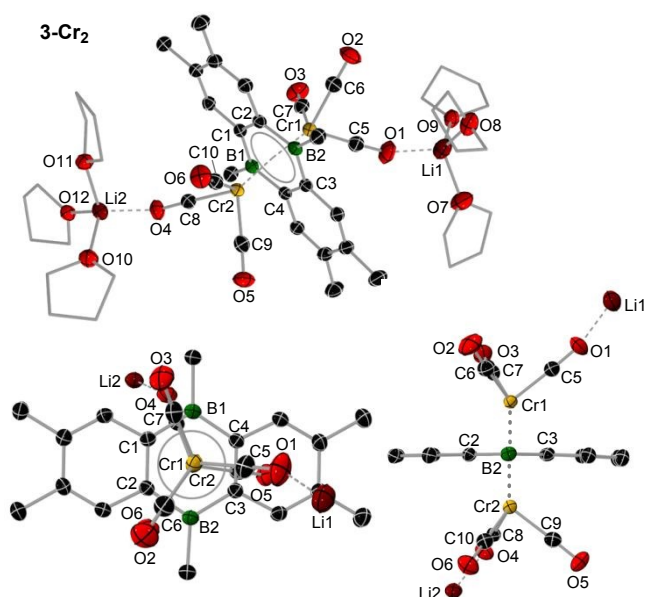


Figure 6. Top: crystallographically determined solid-state structure of **3-Cr₂**. Bottom left: view of **3-Cr₂** (THF ligands omitted) from above the DBA plane, highlighting the eclipsed conformation of the $\text{Cr}(\text{CO})_3$ moieties. Bottom right: truncated view of **3-Cr₂** along the B–B axis (methyl groups and THF omitted), highlighting the planarity of the DBA framework. Thermal displacement ellipsoids set at 50% probability. Hydrogen atoms omitted for clarity.

Complexes 3-M₂. **3-Cr₂** and **3-Mo₂** are isomorphous, crystallising in the $P2_1/c$ space group with near-identical cell parameters ($a \approx 42.0\text{ \AA}$, $b \approx 10.4\text{ \AA}$, $c \approx 24.0\text{ \AA}$, $\beta = 105^{\circ}$). Their asymmetric units contain two crystallographically distinct molecules of **3-M₂**. In each, two $\text{M}(\text{CO})_3$ fragments are η^6 -bound to the central 1,4-DBB ring, while the $\text{Li}(\text{thf})_3$ cations coordinate to one of their CO ligands via Li–O linkages (Figure 6, Table 1, for **3-Mo₂** see Figure S70 in the ESI). Similarly to **3**, the entire [9,10-DBA] $^{2-}$ framework is quasi-planar ($|\omega_{\text{max}}| \leq 2.3(9)^{\circ}$, $\varphi \leq 2.2^{\circ}$). The endocyclic B–C and C–C bond lengths in **3-Cr₂**, **3-Mo₂** are similar within the error of the measurements. Compared to the related neutral diboracene complexes **VI-M** and **VIII-M**,^{21,25} or Roesky's [9,10-DBA] Ln_2 triple-decker complexes,^{27b}

the endocyclic B–C bond lengths in **3-M₂** are slightly longer (ca. 1.55 vs 1.53 \AA), suggesting a slightly lower degree of π conjugation within the C_4B_2 ring. The $\text{Cr}\cdots\text{C}_4\text{B}_2$ distances in **3-M₂** (**3-Cr₂** ca. 1.78 \AA , **3-Mo₂** ca. 1.95 \AA) are shorter than in the corresponding neutral half-sandwich complexes **VIII-M** (ca. 1.80 \AA). In both complexes, the $\text{M}(\text{CO})_3$ units are staggered with respect to the C_4B_2 rings but eclipsed with respect to each other. One of the Li^+ cations coordinates to a CO pointing across one a edge, while the other links to the CO pointing across the e edge, creating an asymmetry between the two sides of the DBA framework. This results in the two metal centres being shifted slightly off-centre, ca. 3% closer to C3–C4 than to the C1–C2 bond. Whereas the terminal CO ligands all show similar C–O bond lengths (avg. $1.173(9)\text{ \AA}$), the Li-bound ones are slightly elongated (avg. $1.194(10)\text{ \AA}$), resulting in the lower wavenumber set of stretching bands observed in the solid-state IR spectra (*vide supra*).

DFT calculations

Compounds 2 and its dianion. In order to quantify the aromaticity changes upon twofold reduction of **2**, nucleus-independent chemical shift (NICS)³⁹ calculations were carried out at the B3LYP-D4-def2-SVP level of theory on the structures of **2** and its naked dianion [**2**] $^{2-}$ (without the $\text{Li}(\text{thf})_2$ moieties) optimised at the $\omega\text{B97X-D4-def2-SVP}$ level of theory (see details in the ESI). Benzene, with a highly negative $\text{NICS}(\pm 1)_{zz}$ value of -29.1 ppm was used as a reference (Table 2).

Table 2. NICS(0), NICS(1) and $\text{NICS}(\pm 1)_{zz}$ (average of $\text{NICS}(1)_{zz}$ and $\text{NICS}(-1)_{zz}$) values (ppm) and C–C/C–B WBIs calculated at the B3LYP-D4-def2-SVP// $\omega\text{B97X-D4-def2-SVP}$ level of theory.

	C_4B_2 ring				C_6 rings				
	NICS (0/1)		WBI		NICS (0/1)		WBI		
		$(\pm 1)_{zz}$	a	e		$(\pm 1)_{zz}$	b	c	d
C_6H_6	–	–	–	–	$-8.9/-11.0$	-29.1	1.41		
2	$10.3/2.4$	$19.7,$ 13.0^a	1.06	1.33	$-4.8/-8.8$	-20.5	1.33	1.39	1.39
[2] $^{2-}$	$-8.2/-11.4$	-32.2	1.33	1.21	$-4.6/-7.4$	-17.5	1.16	1.53	1.20

^a The slight bend in the C_4B_2 ring results in different $\text{NICS}(1)_{zz}$ and $\text{NICS}(-1)_{zz}$ values.

For the two benzo rings the aromaticity decreases slightly upon reduction to the dianion, as seen in their slightly less negative $\text{NICS}(\pm 1)_{zz}$ value (**2** -20.5 ppm ; [**2**] $^{2-}$ -17.5 ppm). In contrast, the central C_4B_2 ring switches from antiaromatic in **2**, with an average positive $\text{NICS}(\pm 1)_{zz}$ value of $+16.6\text{ ppm}$, to highly aromatic in [**2**] $^{2-}$, with a $\text{NICS}(\pm 1)_{zz}$ value of -32.3 ppm , more negative than that of benzene. It is noteworthy that in compound **2** the substantial difference between the $\text{NICS}(-1)_{zz}$ (19.7 ppm) and $\text{NICS}(+1)_{zz}$ (13.0 ppm) values of the C_4B_2 ring is owed to its slightly bent geometry (see **X-ray crystallographic analyses**). For [**2**] $^{2-}$ the $\text{NICS}(-1)_{zz}$ and $\text{NICS}(+1)_{zz}$ values are identical within the error of the calculation, in line with the planarisation of the C_4B_2 ring upon twofold reduction. For comparison, the central ring of the literature-known [9,10-Mes₂-9,10-DBA] $^{2-}$ dianion (Mes = 2,4,6-trimethylphenyl), for which only the $\text{NICS}(0)$ and $\text{NICS}(1)$ values are reported, ($-9.0/-13.1\text{ ppm}$),⁴⁰ is slightly more aromatic than that of [**2**] $^{2-}$ ($-8.2/-$



11.4 ppm). Moreover, the aromatisation of the C_4B_2 ring is also visible in its B–C Wiberg bond indices (WBIs), which increase from 1.06 in **2** (single bonds) to 1.33 in $[2]^{2-}$ (partial double bonds), concomitant with a slight decrease in its C–C WBIs, from 1.33 to 1.21, respectively (Table 2).⁴¹ At the same time the benzo rings lose some of their aromatic character, as seen in the wider range of C–C WBIs ($[2]^{2-}$ 1.16–1.53, **2** 1.33–1.39).

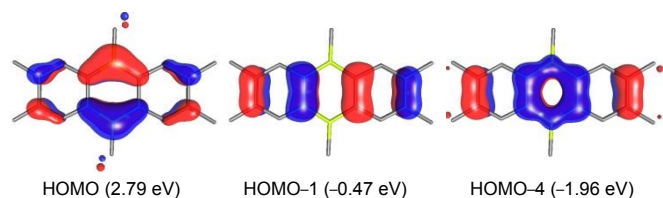


Figure 7. Plots of the frontier MOs of $[2]^{2-}$ involving π delocalisation over the C_4B_2 ring, energy levels in parentheses. Isovalues: 0.04.

The aromatisation of the C_4B_2 ring is also apparent in the frontier MOs. Whereas the π -symmetry HOMOs of **2** are all delocalised over the two benzo rings, the HOMO (which corresponds to the LUMO of **2**), HOMO–1, and HOMO–4 of $[2]^{2-}$ show π delocalisation over the 1,4-diboratabenzene ring akin to that of benzene (Figure 7).

Compounds 2-Cr and 2-Cr₂. Attempts to optimise **2-Cr** and **2-Cr₂** to the geometries observed in the solid state revealed that the various orientations of the $Cr(CO)_3$ unit(s) with respect to 9,10-DHDBA framework are very close in energy (< 1 kcal mol⁻¹) and display very low rotation barriers (< 1 kcal mol⁻¹, see Figure S75 in the ESI). This explains the variety of conformations observed for **2-Cr** and **2-M₂** (M = Cr, Mo, W) in the SCXRD-derived solid-state structures (Figure 4). Furthermore, calculations show that the putative $\eta^6-C_4B_2$ isomer of **2-Cr**, complex **2'-Cr** (see Figure S72 in the ESI), is 22 kcal mol⁻¹ higher in energy than **2-Cr**, thus reflecting the exclusive preference of Cr for η^6 -benzo complexation.

The optimised structures of **2-Cr** and **2-Cr₂** in the solid-state conformations reproduce the slightly off-centre position of the Cr atoms, which are closer to the *e* than *d* edge(s) (Cr–C_d 2.229, Cr–C_e 2.184 Å). A look at the natural bond orbital (NBO)⁴² charges of the benzo rings of **2** (Figure 8a) shows that the *e* edge carbon atoms are significantly more negative (–0.39) than the *d* edge ones (–0.02) due to the polarisation of the benzo π electron density towards the electron-deficient boron atoms (+0.98) of the central ring. This polarisation is also visible in the unsymmetrical π -electron distribution of the HOMO–9 and HOMO–12 (Figure 8b–c), resulting in tighter binding of the Cr centres to the *e* edges in **2-Cr** and **2-Cr₂**.

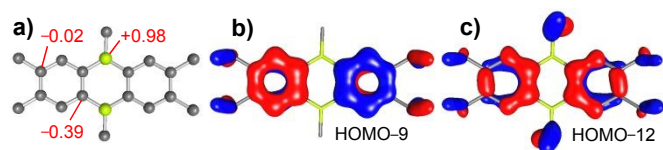


Figure 8. a) Optimised structure of **2** at the ω B97X-D4-def2-SVP level of theory, with NBO charges of the *d* and *e* carbon and boron atoms in red. Atom colours: carbon = grey, boron = green. Hydrogen atoms omitted for clarity. b–c) Plots of the HOMO–9 and HOMO–12 of **2**. Isovalues: 0.04.

Compound 3-Cr₂. The optimised structure of compound **3-Cr₂** starting from the SCXRD-derived solid-state structure reproduces the staggered conformation of the $Cr(CO)_3$ units with respect to the C_4B_2 ring and their eclipsed conformation with respect to each other, as well as the binding of the Li⁺ cations to CO ligands pointing in different directions, and the unsymmetrical positioning of the Cr centres closer to the *e* edges over which the C5–O1...Li1(thf)₃ and C9–O5 carbonyl ligands point. This asymmetry is also visible in the frontier MOs of this structure (see Figure S74 in the ESI). However, since this asymmetry is only present in the solid state, while in solution the $Cr(CO)_3$ moieties rotate freely and the $[Li(thf)_3]^+$ cations fluctuate between all three CO ligands, further calculations were carried out on the dianionic part of **3-Cr₂** ($[3'-Cr_2]^{2-}$) only. Optimisation of several possible conformations of $[3'-Cr_2]^{2-}$ show that that of the solid-state conformation of $[3'-Cr_2]^{2-}$ is the overall minimum. The HOMO and HOMO–2 to HOMO–5 of $[3'-Cr_2]^{2-}$ are entirely $Cr(CO)_3$ -based, while HOMO–6 to HOMO–10, HOMO–16 and HOMO–18 essentially correspond to the π -delocalised orbitals of the anion $[2]^{2-}$, each with very small σ -bonding contributions to the matching chromium d orbitals. Only the HOMO–1 and HOMO–6 present significant σ bonding between the chromium d orbitals and the B–C π bonds of one half of the C_4B_2 ring, respectively (Figure 9).

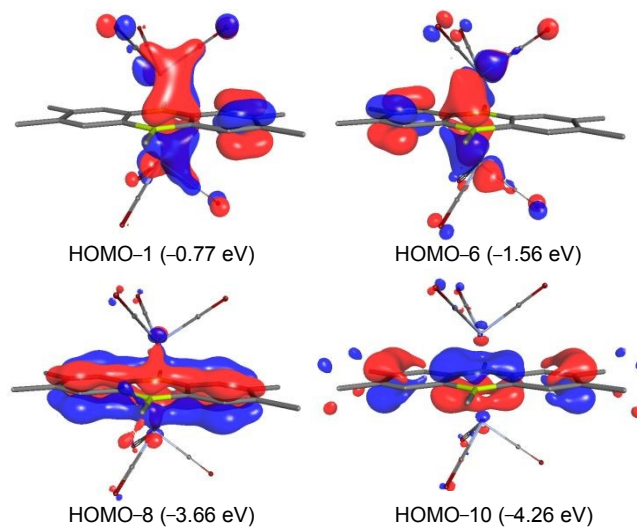


Figure 9. Plots of the frontier MOs of $[3'-Cr_2]^{2-}$ involved in $Cr \cdots C_4B_2$ bonding. Energy levels in parentheses. Isovalues: 0.04.

An intrinsic bonding orbital (IBO)⁴³ analysis shows three IBOs involved in $Cr \cdots C_4B_2$ bonding (Figure 10). IBO-1 and IBO-2 involve σ donation from essentially the B1–C4 (68% contribution) and C1–C2 (75%) π bonds into the two chromium d_{xz} orbitals (6%, respectively), while IBO-3 involves donation from the B2–C3 π bond (68%) into the chromium d_{yz} orbitals (8%). It is noteworthy that the contribution of each boron 2p_z orbital to these three IBOs (ca. 24%) is significantly lower than that of each carbon one (ca. 40% for C1/C2, ca. 50% for C3/C4). The rather low chromium contributions ($\leq 4\%$ per Cr) to these IBOs suggest that the $Cr^0 \leftarrow [2]^{2-} \rightarrow Cr^0$ interaction is mainly electrostatic in nature. Interestingly, an atoms-in-molecules



(AIM)⁴⁴ analysis provides bond critical points (BCP) only for the Cr–C bonds, and none for the Cr···B interactions (see Figure S76 in the ESI).

ring in **3-M₂** is mainly electrostatic in nature, without formal Cr–B bonding.
DOI: 10.1039/D6SC02501C

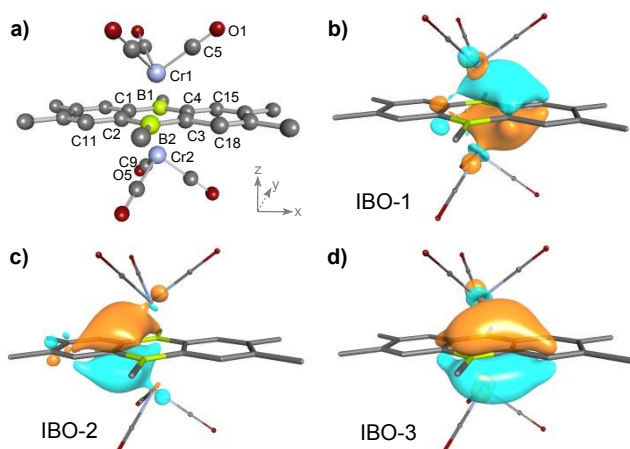


Figure 10. a) Optimised structure of $[3'-\text{Cr}_2]^{2-}$ at the $\omega\text{B97X-D4-def2-SVP}$ level of theory. The hydrogen atoms and $\text{Li}(\text{thf})_3$ moieties have been omitted for clarity. b-d) IBOs of $[3'-\text{Cr}_2]^{2-}$ involved in Cr···C₄B₂ bonding. Main orbital contributions to IBO-1: 21% $2p_z(\text{B1})$, 47% $2p_z(\text{C4})$, 4% $2p_z(\text{C15})$, 4% $2p_z(\text{C3})$, 2% $2p_z(\text{C2})$, 3% $3d_{xz}(\text{Cr2})$, 2% $3d_{xz}(\text{Cr1})$; to IBO-2: 4% $2p_z(\text{B1})$, 40% $2p_z(\text{C1})$, 35% $2p_z(\text{C2})$, 2% $2p_z(\text{B2})$, 1% $3d_{xz}(\text{Cr1})$, 1% $3d_{xz}(\text{Cr2})$; to IBO-3: 2% $2p_z(\text{C2})$, 22% $2p_z(\text{B2})$, 46% $2p_z(\text{C3})$, 3% $2p_z(\text{C18})$, 3% $2p_z(\text{C4})$, 4% $3d_{yz}(\text{Cr1})$, 4% $3d_{yz}(\text{Cr2})$. Isovalues: 0.04.

Conclusions

We have shown that the neutral 9,10-DHDBA **2** and its doubly reduced $[9,10\text{-DBA}]^{2-}$ dilithio inverse-sandwich complex **3** are suitable precursors for the complexation of group 6 carbonyls. While compound **2** forms a stable, unsymmetrical half-sandwich complex (**2-Cr**) by coordination of $\text{Cr}(\text{CO})_3$ to one of the benzo rings, the analogous Mo and W complexes are not accessible. DFT calculations show that coordination to the central C₄B₂ ring is disfavoured by 22 kcal mol⁻¹. In contrast, all three group 6 metals form stable centrosymmetric slipped inverse-sandwich complexes (**2-M₂**, M = Cr, Mo, W) by coordination of one $\text{M}(\text{CO})_3$ to each benzo ring, one above and one below the DHDBA plane. These all display a slightly bent DHDBA framework, with the metal centres coordinating more tightly to the ring junctions, where π density accumulates due to the attraction exerted by the central electrophilic boron atoms.

Twofold reduction of **2** with lithium yields the inverse-sandwich complex **3**, in which the two lithium cations coordinate to either side of the now aromatic central 1,4-diborabenzene ring. While **3** is only stable in solution, its reaction with $[\text{M}(\text{CO})_3(\text{NMe})_3]$ (M = Cr, Mo) yielded the first stable zerovalent TM inverse-sandwich complexes of a diborataanthracene ligand (**3-M₂**, M = Cr, Mo), albeit in poor yields. SCXRD analyses confirm that the two $\text{M}(\text{CO})_3$ units bind in an η^6 fashion to the central C₄B₂ ring of the DBA dianion, while the $[\text{Li}(\text{thf})_3]^+$ counteranions bind to one CO ligand of each $\text{M}(\text{CO})_3$ unit. Finally, DFT calculations show that $\text{M}(\text{CO})_3$ bonding to the central 1,4-diborabenzene

Conflicts of interest

There are no conflicts to declare.

Acknowledgements

The authors gratefully acknowledge funding from the Deutsche Forschungsgesellschaft (DFG grants BR1149/30-1 466754611) and a Fonds der Chemischen Industrie (FCI) Kékulé stipend for AG.

Notes and references

† There is one important difference: whereas 9,10-Br₂-9,10-DHDBA only forms under static reduced pressure (i.e. evacuation of the headspace of the flask prior to heating), **1** only forms under elevated pressure. Under static reduced pressure, the reaction yields 1,2-bis(dibromoboryl)-4,5-dimethylbenzene instead.

- 1 a) T. J. Kealy and P. L. Pauson, *Nature*, 1951, **168**, 1039–1040; E. O. Fischer and W. U. Hafner, *Z. Naturforsch. B*, 1955, **10**, 665–668.
- 2 a) U. Rosenthal, *Angew. Chem. Int. Ed.*, 2018, **57**, 14718–14735; b) L. Becker and U. Rosenthal, *Coord. Chem. Rev.*, 2017, **345**, 137–149; c) S. Schäfer, S. Kaufmann, E. S. Rösch and P. W. Roesky, *Chem. Soc. Rev.*, 2023, **52**, 4006–4045; d) P. J. Chirik, *Organometallics*, 2010, **29**, 1500–1517.
- 3 a) A. Desgranges, F. D'Agosto and C. Boisson, *ChemPlusChem*, 2024, **89**, e202400262; b) J. Okuda, *J. Organomet. Chem.*, 2023, **1000**, article 122833; c) *Metalloocene Complexes as Catalysts for Olefin Polymerization*, ed. H. G. Alt, *Coord. Chem. Rev.*, 2006, **250**, 1–272.
- 4 a) T. Wang and D. Astruc, *Coord. Chem. Rev.*, 2025, **524**, article 216300; b) M. V. Kharlamova and C. Kramberger, *Nanomater.*, 2023, **13**, article 774; c) A. Zabala-Lekuona, J. M. Seco and E. Colacio, *Coord. Chem. Rev.*, 2021, **441**, article 213984; d) H. Gu, R. Ciganda, S. Gatard, F. Lu, P. Zhao, J. Ruiz and D. Astruc, *J. Organomet. Chem.*, 2016, **821**, 54–61; e) D. Astruc, C. Ornelas and J. Ruiz, *Chem. Eur. J.*, 2009, **15**, 8936–8944.
- 5 a) A. Kalamatianou, C. Ludwig, S. Zhong, K. Cariou and G. Gasser, *Chem. Soc. Rev.*, 2025, **54**, 3930–3961; b) I. Kostova, *Molecules*, 2024, **29**, article 824; c) M. M. Santos, P. Bastos, I. Catela, K. Zalewska and L. C. Branco, *Mini-Rev. Med. Chem.*, 2017, **17**, 771–784.
- 6 a) D. Patel, J. McMaster, W. Lewis, A. J. Blake, S. T. Liddle, *Nat. Commun.*, 2013, **4**, article 2323; b) C. Yu, B. Wu, Z. Yang, H. Chen, W.-X. Zhang and Z. Xi, *Bull. Chem. Soc. Jpn.*, 2020, **93**, 1314–1318; c) A. Sekiguchi, T. Matsuo and H. Watanabe, *J. Am. Chem. Soc.*, 2000, **122**, 5652–5653.
- 7 a) D. Jędrzkiewicz, M. Morasch, O. P. E. Townrow, B. Rösch, J. Langer, Z. Mathe and S. Harder, *Chem. Sci.*, 2025, **16**, 17793–17802; b) Y. Wang, R. Sun, J. Liang, Y. Zhang, B. Tan, C. Deng, Y.-H. Wang, B.-W. Wang, S. Gao and W. Huang, *J. Am. Chem. Soc.*, 2025, **147**, 7741–7748; c) F. Delano IV and S. Demir, *Angew. Chem. Int. Ed.*, 2025, **64**, e202417217; d) C. A. Gould, J. Marbey, V. Vieru, D. A. Marchiori, R. D. Britt, L. F. Chibotaru, S. Hill and J. R. Long, *Nature Chem.*, 2021, **13**, 1001–1005; e) P. L. Arnold, S. M. Mansell, L. Maron and D. McKay, *Nature Chem.*, 2012, **4**, 668–674; f) P. L. Diaconescu, P. L. Arnold, T. A. Baker, D. J. Mindiola and C. C. Cummins, *J. Am. Chem. Soc.*, 2000, **122**, 6108–6109.



- 8 a) M. Liu, Y.-C. Chen, A. Mondal, H. Wang, M.-L. Tong, R. A. Layfield and F.-S. Guo, *J. Am. Chem. Soc.*, 2025, **147**, 11359–11367; b) K. R. McClain, A. H. Vincent, A. Rajabi, D. X. Ngo, K. R. Meihaus, F. Furche, B. G. Harvey and J. R. Long, *J. Am. Chem. Soc.*, 2024, **146**, 32708–32716; c) Y. Wang, Y. Zhang, J. Liang, B. Tan, C. Deng and W. Huang, *Chem. Sci.*, 2024, **15**, 8740–8749 (correction: *Chem. Sci.*, 2024, **15**, 10669–10669); d) W. Huang, F. Dulong, T. Wu, S. I. Khan, J. T. Miller, T. Cantat, P. L. Diaconescu, *Nature Commun.*, 2013, **4**, article 1448; e) S. Kriek, H. Görls, L. Yu, M. Reiher and M. Westerhausen, *J. Am. Chem. Soc.*, 2009, **131**, 2977–2985
- 9 a) M. S. Hill, M. F. Mahon, A. S. S. Wilson, C. Dinoi, L. Maron and E. Richards, *Chem. Commun.*, 2019, **55**, 5732–5735; b) P. L. Diaconescu and C. C. Cummins, *J. Am. Chem. Soc.*, 2002, **124**, 7660–7661; c) H. Schumann, J. Winterfeld, L. Esser and G. Kociok-Köhn, *Angew. Chem. Int. Ed. Engl.*, 1993, **32**, 1209–1210.
- 10 S. T. Liddle, *Coord. Chem. Rev.*, 2015, **293–294**, 211–227.
- 11 V. Beck and D. O'Hare, *J. Organomet. Chem.*, 2004, **689**, 3920–3938.
- 12 a) T. L. Gianetti, G. Nocton, S. G. Minasian, N. C. Tomson, A. L. D. Kilcoyne, S. A. Kozimor, D. K. Shuh, T. Tyliczszak, R. G. Bergman and J. Arnold, *J. Am. Chem. Soc.*, 2013, **135**, 3224–3236; b) Y.-C. Tsai, P.-Y. Wang, S.-A. Chen and J.-M. Chen, *J. Am. Chem. Soc.*, 2007, **129**, 8066–8067; c) W. H. Monillas, G. P. A. Yap and K. H. Theopold, *Angew. Chem. Int. Ed.*, 2007, **46**, 6692–6694; d) Y.-C. Tsai, P.-Y. Wang, K.-M. Lin, S.-A. Chen and J.-M. Chen, *Chem. Commun.*, 2008, 205–207.
- 13 a) Y.-S. Huang, G.-T. Huang, Y.-L. Liu, J.-S. K. Yu and Y.-C. Tsai, *Angew. Chem. Int. Ed.*, 2017, **56**, 15427–15431.
- 14 C. Ni, B. D. Ellis, J. C. Fettingner, G. J. Long and P. P. Power, *Chem. Commun.*, 2008, 1014–1016.
- 15 a) G. C. Bazan, W. D. Cotter, Z. J. A. Komon, R. A. Lee and R. J. Lachicotte, *J. Am. Chem. Soc.*, 2000, **122**, 1371–1380; b) Herberich and D. Söhnen, *J. Organomet. Chem.*, 1983, **254**, 143–147; c) D. W. Clack and K. D. Warren, *Inorg. Chem.*, 1979, **18**, 513–519.
- 16 a) R. Wang, C.-S. Lee and Z. Lu, *J. Organomet. Chem.*, 2023, **984**, article 122564; b) K. Rojas, M. Tamizmani, T. A. Bartholome and C. D. Martin, *Dalton Trans.*, 2022, **51**, 17216–17223; c) J. He, F. Rauch, M. Finze and T. B. Marder, *Chem. Sci.*, 2021, **12**, 128–147; d) S. K. Mellerup and S. Wang, *Trends Chem.*, 2019, **1**, 77–89; e) E. von Grothuss, A. John, T. Kaese and M. Wagner, *Asian J. Org. Chem.*, 2018, **7**, 37–53.
- 17 a) P. Cui and Y. Chen, *Coord. Chem. Rev.*, 2016, **314**, 2–13; b) A. J. Ashe, III, *Organometallics*, 2009, **28**, 4236–4248; c) G. C. Fu, *Adv. Organomet. Chem.*, 2001, **47**, 101–119; d) G. E. Herberich and H. Ohst, *Adv. Organomet. Chem.*, 1986, **25**, 199–236.
- 18 V. Pérez, S. S. Barnes and F.-G. Fontaine, *Eur. J. Inorg. Chem.*, 2014, 5698–5702.
- 19 G. E. Herberich, J. Hengesbach, G. Huttner, A. Frank and U. Schubert, *J. Organomet. Chem.*, 1983, **246**, 141–149.
- 20 a) T. Heitkemper, J. Sarcevic and C. P. Sindlinger, *J. Am. Chem. Soc.*, 2020, **142**, 21304–21309; b) G. E. Herberich, I. Hausmann, B. Hessner and M. Negele, *J. Organomet. Chem.*, 1989, **362**, 259–264.
- 21 J. Böhnke, H. Braunschweig, J. O. C. Jiménez-Halla, I. Krummenacher and T. E. Stennett, *J. Am. Chem. Soc.*, 2018, **140**, 848–853.
- 22 M. Dietz, M. Arrowsmith, S. Reichl, L. I. Lugo-Fuentes, J. O. C. Jiménez-Halla, M. Scheer and H. Braunschweig, *Angew. Chem. Int. Ed.*, 2022, **61**, e202206840.
- 23 M. Dietz, M. Arrowsmith, L. Endres, V. Paprocki, B. Engels and H. Braunschweig, *J. Am. Chem. Soc.*, 2023, **145**, 22222–22231.
- 24 T. Zhao, Y. Dai, P. Cui, C.-H. Tung and L. Kong, *J. Am. Chem. Soc.*, 2025, **147**, 40113–40119.
- 25 M. Dietz, M. Arrowsmith and H. Braunschweig, *Dalton Trans.*, 2024, **53**, 449–453. View Article Online
DOI: 10.1039/D6SC02501C
- 26 a) A. Lorbach, M. Bolte, H.-W. Lerner, M. Wagner, *Organometallics*, 2010, **29**, 5762–5765; b) C. Balzereit, H.-J. Winkler, W. Massa and A. Berndt, *Angew. Chem. Int. Ed. Engl.*, 1994, **33**, 2306–2308; c) G. E. Herberich, B. Hessner and M. Hostalek, *Angew. Chem. Int. Ed. Engl.*, 1986, **25**, 642–643.
- 27 a) M. Tamizmani, J. R. Tidwell, E. W. Reinheimer, B. M. Lindley and C. D. Martin, *Inorg. Chem.*, 2023, **62**, 7150–7154; b) C. Uhlmann, L. Münzfeld, A. Hauser, T.-T. Ruan, S. Kumar Kuppusamy, C. Jin, M. Ruben, K. Fink, E. Moreno-Pineda and P. W. Roesky, *Angew. Chem. Int. Ed.*, 2024, **63**, e202401372; c) G. E. Herberich and B. Heßner, *Chem. Ber.*, 1982, **115**, 3115–3127.
- 28 P. Müller, S. Hucka, H. Köppel, H. Pritzkowa and W. Siebert, *Z. Naturforsch.*, 1995, **50b**, 1476–1484.
- 29 E. Januszewski, A. Lorbach, R. Grewal, M. Bolte, J. W. Bats, H.-W. Lerner and M. Wagner, *Chem. Eur. J.*, 2011, **17**, 12696–12705.
- 30 E. von Grothuss, S. E. Prey, Michael Bolte, H.-W. Lerner and M. Wagner, *Angew. Chem. Int. Ed.*, 2018, **57**, 16491–16495.
- 31 P. Müller, B. Gangnus, H. Pritzkow, H. Schulz, M. Stephan and W. Siebert, *J. Organomet. Chem.*, 1995, **487**, 235–243.
- 32 a) H. Schulz, H. Pritzkow and W. Siebert, *Chem. Ber.*, 1991, **124**, 2203–2207; b) P. Müller, H. Pritzkow and W. Siebert, *J. Organomet. Chem.*, 1996, **524**, 42–47.
- 33 B. E. Mann, *Chem. Commun.*, 1971, 976–977.
- 34 R. D. Fischer, *Chem. Ber.*, 1960, **93**, 165–175.
- 35 F. Hanic and O. S. Mills, *J. Organomet. Chem.*, 1968, **11**, 151–158.
- 36 M. Trömel, *Z. Naturforsch.*, 2000, **55b**, 243–247.
- 37 a) M. F. Bailey and L. F. Dahl, *Inorg. Chem.*, 1965, **4**, 1314–1319; b) H.-B. Bürgi, A. Raselli, D. Braga and F. Grepioni, *Acta Cryst. B*, 1992, **48**, 428–437; c) J. M. Oh, S. J. Geib and N. J. Cooper, *Acta Cryst. C*, 1998, **54**, 581–583.
- 38 a) E. von Grothuss, M. Diefenbach, M. Bolte, H.-W. Lerner, M. C. Holthausen and M. Wagner, *Angew. Chem. Int. Ed.*, 2016, **55**, 14067–14071; b) E. von Grothuss, S. E. Prey, M. Bolte, H.-W. Lerner and M. Wagner, *J. Am. Chem. Soc.*, 2019, **141**, 6082–6091.
- 39 a) Z. Chen, C. S. Wannere, C. Corminboeuf, R. Puchta and P. von Ragué Schleyer, *Chem. Rev.*, 2005, **105**, 3842–3888; b) A. Stanger, *J. Org. Chem.*, 2006, **71**, 883–893.
- 40 C. Hoffend, M. Diefenbach, E. Januszewski, M. Bolte, H.-W. Lerner, M. C. Holthausen and M. Wagner, *Dalton Trans.*, 2013, **42**, 13826–13837.
- 41 K. B. Wiberg, *Tetrahedron*, 1968, **24**, 1083–1096.
- 42 A. E. Reed, R. B. Weinstock and F. Weinhold, *J. Chem. Phys.*, **1985**, **83**, 735–746.
- 43 G. Knizia, *J. Chem. Theory Comput.*, 2013, **9**, 4834–4843.
- 44 R. F. W. Bader, *Int. Ser. Monogr. Chem.*, Oxford University Press: Oxford, UK, 1990, Vol. **22**.



The data supporting the findings are included in the Supporting Information. Crystallographic data has been deposited at the Cambridge Crystallographic Data Center as supplementary publication with deposition numbers 2538786-2538794.

